Heliyon 8 (2022) e09032

Contents lists available at ScienceDirect

Heliyon

journal homepage: www.cell.com/heliyon

Research article

Mesostructural study on graphenic-based carbon prepared from coconut shells by heat treatment and liquid exfoliation

Deril Ristiani [a], Retno Asih [a], Fahmi Astuti [a], Malik Anjelh Baqiya [a], Chonthicha Kaewhan [b], Sarayut Tunmee [b], Hideki Nakajima [b], Siriwat Soontaranon [b], Darminto [a,*]

[a] Department of Physics, Faculty of Science and Data Analytics, Institut Teknologi Sepuluh Nopember, Surabaya 60111, Indonesia
[b] Synchrotron Light Research Institute, 111 University Venue, Muang District, Nakhon Ratcashima 30000, Thailand

ARTICLE INFO

Keywords:
Carbon
Coconut shell
Graphenic
Mesostructure
Heat treatments
SAXS

ABSTRACT

In this study, the effect of heating temperature on the structure of graphenic-based carbon (GC) has been successfully investigated. A series of GC materials was prepared from coconut shells by a green synthesis method. The process includes heating at four temperatures (T = 400, 600, 800 and 1000 °C) followed by an exfoliation process assisted by hydrochloric acid (HCl). These materials were characterized by wide- and small-angle x-ray scattering (WAXS and SAXS), Fourier-transform infrared spectroscopy (FTIR), x-ray photoemission spectroscopy (XPS) and transmission electron microscopy (TEM). The WAXS analysis shows Braggs peaks corresponding to the reduced graphene oxide (rGO)-like phase. Investigations by FTIR and XPS methods show the presence of carbon-oxygen functional groups such as C=C (carbon with sp^2 hybridization), C–C (carbon with sp^3 hybridization), and C=O bonds. The sp^2 bonds form a 2-dimensional (2D) network in hexagonal lattice, while carbon with sp^3 bonds tends to form a 3-dimensional (3D) tetrahedral structure. The BET analysis revealed meso- and micro-pore structures in GC. Heating process reduces the specific surface area and increases pore size of GC. Moreover, increasing the heating temperature induces a decrease in radius of gyration (R_g) and an increase in the formation of 2D structures in GC. The fitting results of SAXS profiles, proved by TEM and XPS, yielded the structure of GC containing the mixture of 2D and 3D structures. Thus, it is suggested that the GC has a mesostructure.

1. Introduction

Since the discovery of graphene by Novoselov and Geim, it has attracted huge interest in the science of carbon materials [1]. As a new material, the use of graphene is remarkable because of its superior mechanical, thermal, electric, and magnetic properties [2]. Graphene is a two-dimensional layered material consisting of carbon atoms arranged in a honeycomb lattice [3]. When oxidized, it forms graphene oxide (GO), in which various oxygen-containing functionalities are present [4]. Further, GO can be reduced to become reduced graphene oxide (rGO): a promising material for various applications, such as high capacity energy storage [5, 6], sensors [7], super capacitors [8], solar cell applications [9], hybrid electrocatalysts [10], high-performance electrode materials [11], microwave absorber [12, 13], and medical applications [14]. Due to potential applications of GC, it is important to understand its structure. Its physical and mechanical properties are suggested to strongly depend on its structure, including size and shape. For that reason, a more detailed investigation of the GC structure is necessary to obtain its expected properties.

Currently, an environmentally friendly starting material to produce graphene-based materials is more preferred. In nature, there are many sources of carbon, most of which originate from mining activities such as graphite, coal, and diamond as well as natural gas and liquid hydrocarbon sources (oil and gas). Carbon compounds from mining materials are categorized as non-renewable and non-environmentally friendly resources. Meanwhile, natural carbon sources are also available in the form of biomaterials derived from plants, either as products (bio-products) or waste (bio-waste), which are more environmentally friendly. An rGO-like structure has been found standing on natural carbon sources, coconut shell charcoal, by the facile synthesis, including the heating and the exfoliation processes [15, 16, 17, 18]. Differences in synthesis route and treatment provide a unique and different nature of the obtained rGO [2]. Various synthesis methods have been performed to yield rGO, such as epitaxial growth [19], chemical vapor deposition (CVD) [20], hydrothermal [21], and mechanical, thermal and chemical exfoliations [22].

* Corresponding author.
E-mail address: darminto@physics.its.ac.id (Darminto).

https://doi.org/10.1016/j.heliyon.2022.e09032
Received 7 October 2021; Received in revised form 27 January 2022; Accepted 24 February 2022

Chemical exfoliation and thermal methods are the most widely used since they are easy to synthesize and controllable [23]. A. V. Dolbin et al. investigated the effect of the thermal reduction temperature on rGO and revealed that the reduction temperature affects the final oxygen content and creates structural damage by removing water and oxygen functionalities from the surface [24]. They also clearly state that high temperature treatments contribute to restore sp^2 hybridized bonds. In addition, S. Farah et al. stated that the oxygen functionalities could be partially removed and create further defects by both thermal and chemical reduction methods [22]. Therefore, controlling the structure of graphene during its synthesis treatments is the key in preparing materials for many applications.

In the present work, graphenic-based carbon (GC) was produced using coconut shells as starting materials. Both the thermal and hydrochloric acid-assisted chemical exfoliation methods was applied for this production. It has been reported that the heating process, followed by the exfoliation process, is effective in exfoliating and breaking the van der Waals bonds between carbon layers [17, 24]. The use of hydrochloric acid has also been proven to reduce the particle size of graphene [17]. In this study, the heating process was carried out at temperatures ranging from 400 to 1000 °C to observe changes in the structure of the obtained GC. In a study conducted by M. A. Baqiya et al., the x-ray diffraction (XRD) and FTIR characterization show the formation of an rGO-like structure, and the presence of molecular bonds such as C=C, C–C, C–H, C–O, C=O, and O–H prove the formation of the rGO-like structure [15, 16, 17, 18]. Beyond XRD, here, WAXS measurement is performed to investigate the structure and phases of the obtained GC particles. WAXS is an x-ray technique typically employed to analyze the crystallinity in polymer systems [25, 26]. Graphene has been surface-characterized using some material characterization techniques such as transmission electron microscopy (TEM) and atomic force microscopy (AFM) [17, 27]. All these types of structural characterization only explain qualitatively and lack explanation regarding structural quantification. SAXS is a well-known quantitative technique that can complement AFM, TEM, and other surface characterization techniques [28, 29]. The SAXS technique can give an average value of the size of sheets. It has been used earlier for analyzing the structure of graphene-based particles prepared from coconut shell charcoal and revealed that the structure contains some particles formed as spherical and agglomerated plate-like flakes with a nano-sized radius [17]. However, structural quantification for bigger structures is not detailed yet. Therefore, a better model is proposed for detailing and analyzing the structure of GC.

2. Experimental

2.1. Materials

In this study, the materials used were old coconut shells and hydrochloric acid (HCl). Waste of old coconut shells was collected from local food market in Indonesia. The HCl (ACS reagent, 37%) is supplied from Merck India Ltd.

2.2. Synthesis of GC

Firstly, old coconut shells were cleaned, dried, and burned to obtain charcoal. The charcoal was then crushed and sieved to obtain fine charcoal powder with a homogeneous particle size. The charcoal powder was heated with temperature variations of 400, 600, 800, and 1000 °C for 5 h to obtain GC powder. A liquid-based exfoliation technique was used to release stacked GC sheets [15, 16, 17, 18]. This exfoliation process was assisted by HCl during bath sonication. The first step was to make a GC solution by dispersing 4 g of GC powder into 100 ml of 1M HCl solution. The solution then was stirred for 24 h at temperature of 80 °C using a magnetic stirrer. The solution obtained was directly ultra-sonicated for 10 h at room temperature. To separate the deposits from the liquid part, the solution was centrifuged for 30 min at 3000 rpm. The deposits were then dried using a hot plate at a temperature of 100 °C for 5 h. These powders are labeled as GC400, GC600, GC800, and GC1000 (GC means graphene-based carbon, and the numbers indicate heating temperatures). To aid comprehension, a simple schematic that summarizes the entire synthesis process is presented in Figure 1.

2.3. Characterization

Thermal analysis utilizing METTLER TOLEDO TGA (thermogravimetric analysis) was used to investigate the decomposition characteristics of coconut shells. Structural characterization of the GC was analyzed by WAXS diffraction patterns in the 2θ range of 10–55°. The WAXS patterns of the GC powders were collected at the Siam Photon Laboratory (SPL) of the Synchrotron Light Research Institute (SLRI), Thailand, using Beamline 1.3W. The WAXS patterns were displayed in two-dimensional (2D) scattering intensity maps, then converted and presented as scattering intensity $I(q)$ vs. the angle between the incident and the diffracted x-ray (2θ). Fourier transform infrared spectroscopy (FTIR) measurements were conducted by the Shimadzu 8400S series in the wavenumber range of 400–4000 cm^{-1}. The chemical composition and chemical bonding of the GC was characterized using the X-ray photoelectron spectroscopy (XPS) technique at Beamline 3.2Ua (BL3.2Ua) of the SLRI, Thailand. Raman spectroscopy (RAMAN iHR320 HORIBA) was also used to qualitatively assess the defects in the materials. This measurement is critical for determining the disorder structures present in carbon-based materials. The Brunauer-Emmett-Teller (BET) model was used to analyze the specific surface area and pore size distribution utilizing the Quantachrome Novatouch Lx4 instrument. The surface microstructure and morphology of GC was characterized using Scanning and Transmission Electron Microscopy (SEM, Zeiss EVO MA10 and TEM, Hitachi HT7700 operating at 120kV), respectively. In order to investigate the size and shape of the GC, Small angle x-ray scattering (SAXS) measurements were carried out in the beamline BL1.3 W of the SLRI. SAXS, an important non-destructive tool for characterizing materials, has electron density fluctuation on the length scale of about 1–100 nm [17].

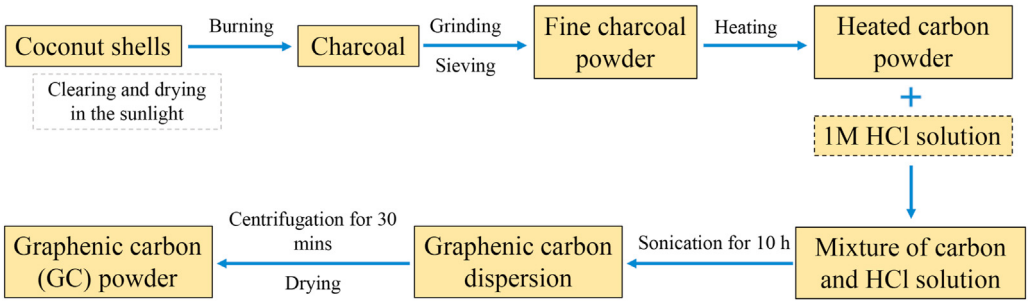

Figure 1. A schematic diagram of fabricating GC from old coconut shells using heat treatments and HCl-assisted exfoliation techniques.

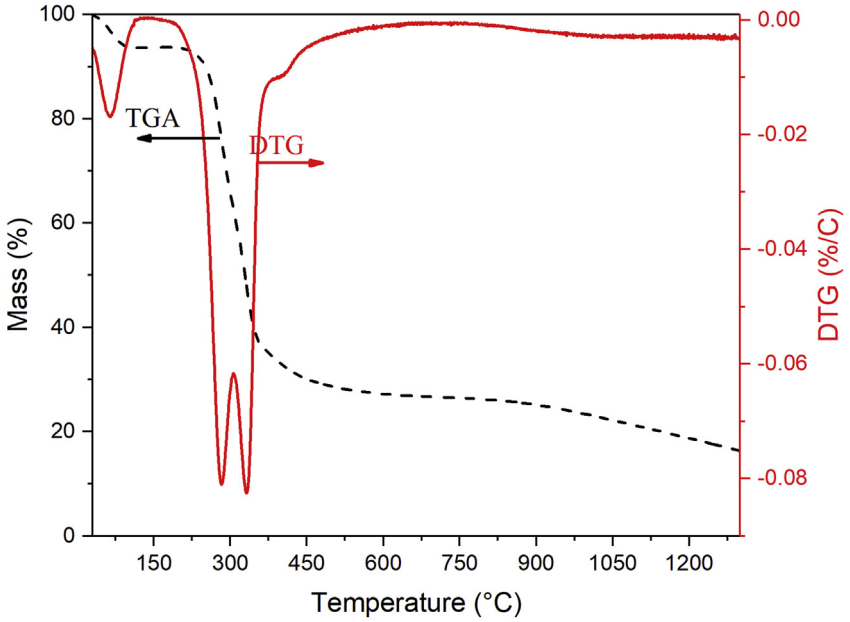

Figure 2. TGA and its corresponding DTG curve of coconut shells.

3. Results and discussion

The thermal analysis of coconut shells using TGA is shown in Figure 2. It can be used to estimate the thermal decomposition behavior of biomass as a function of weight reduction (TGA curve) and its first derivative (DTG - derivative thermogravimetric curve). A minor peak was observed in the DTG curve at temperatures below 100 °C, which corresponds to the release of intrinsic water [30, 31], resulting in an approximate mass loss of 5.7%. A significant amount of mass loss (~45.26 %) occurs between 200 and 400 °C. Generally, heat degradation of biomass occurs as a result of hemicellulose, cellulose, and lignin decomposition [32, 33]. Two distinct peaks at 283.50 and 336.78 °C can be associated with the decomposition of hemicellulose and cellulose content in coconut shells, respectively [30] which results in a weight loss of approximately 22.87% and 22.39%. Slow degradation occurs at temperatures greater than 400 °C and continues up to 1300 °C with a weight loss of 16.36%. This can be attributed to lignin decomposition and the degradation of certain oxygen functional groups [30].

Figure 3 shows WAXS patterns of GC. WAXS is a diffraction-based technique that can be used to investigate crystal structure and orientation and to verify the average distance between graphenic layers [34, 35].

The WAXS pattern shows that the appearance of two broad peaks at positions ~23° and ~43° correspond to the (002) plane and the (100) plane, respectively. It indicates the characteristics of a pristine rGO phase. The broad peaks may be attributed to the arrangement of the graphene layers, which tend to be random along the stacking direction of graphene sheets. This implies that the GC has peeled off into one or only few graphene layers with a lattice spacing of 0.39 nm. This is significantly greater than the lattice spacing in graphite with a value of approximately 0.33 nm. It indicates that the graphene layers are well-separated and not stacked as in graphite [36]. Furthermore, as temperature increases, a more intense peak at (100) plane is observed. This could be associated with a reduction of oxygen functional groups and defects in the sample, which would be further confirmed using FTIR analysis.

FTIR spectra of GC are presented in Figure 4, showing the presence of similar types of molecular bonds/functional groups in all of the samples. The molecular bonds that appear are indicated by the presence of the transmittance peaks of the FTIR pattern. Each molecular bond has a different wave number based on the ability of the molecular bonds to vibrate and absorb energy from the infrared spectrum. The results of the FTIR pattern of all samples qualitatively show that the main molecular bonds on rGO were identified, such as C=C and C–O bonds. Both of them bond together to form the hexagonal structure of the carbon atoms which are arranged into the rGO layer. Transmittance peaks in the FTIR spectrum of GC observed at ~1696 cm^{-1} that corresponds to C=O/carbonyl stretching vibrations, those at ~1550 cm^{-1} that denotes C=C stretching vibrations, ~1107 cm^{-1} that represents stretching vibrations from C–O, and ~871 cm^{-1} that is assigned as C–H/hydrocarbyl vibrations [17, 37]. It is noticeable that the absorption intensity of some oxygen functional groups decreases with increasing the heating temperature. This confirms the WAXS results, in which as the temperature increases, the detected peak of the (100) plane gets more intense. Thus, it can be assumed that the more intense peak in (100) plane is due to the decreased oxygen functional group. A deeper analysis using x-ray photoemission spectroscopy (XPS) will be quite useful to confirm the moieties present in the samples.

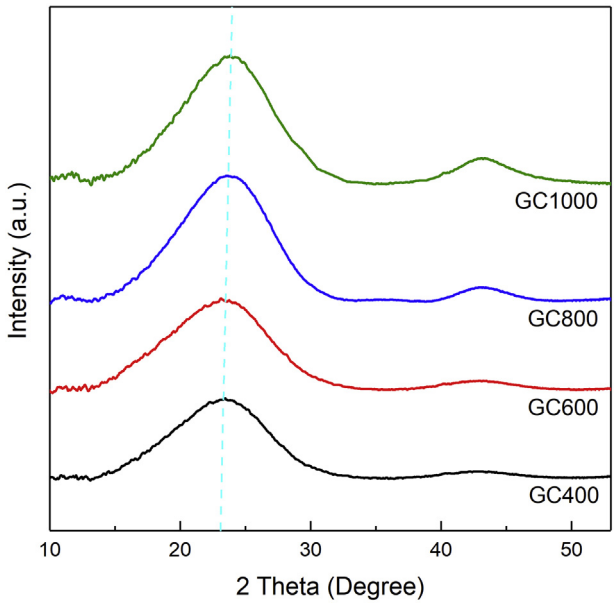

Figure 3. WAXS spectra of the GC samples.

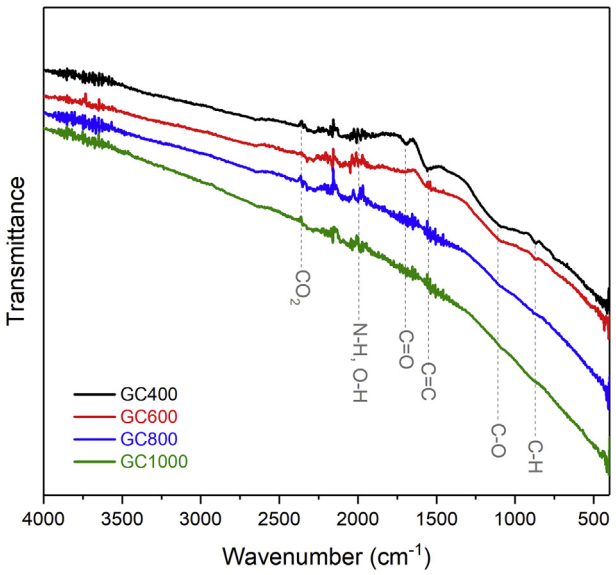

Figure 4. FTIR spectra of the GC samples.

XPS is a spectroscopic technique used for quantitative surface analysis. It can provide chemical information on the sample, such as elemental composition, impurities, empirical formula and electronic state of the element [38, 39]. In this study, XPS was performed to measure the chemical bonding and sp^2/sp^3 ratio in GC. The high-resolution C1s and O1s spectra of the obtained GC are presented in Figure 5 (a) and (b), respectively. The C1s and O1s spectra were fitted by the Gaussian function and the Shirley background correction. Deconvolution was performed using Microsoft Excel equipped with macros software. The C1s spectra were deconvoluted into three component peaks attributed to carbon with sp^2 hybridization (C=C) at ~284 eV, carbon with sp^3 hybridization (C–C) at ~285 eV, and the carbonyl carbon (C=O) at ~288 eV [40, 41]. The O1s spectral peaks show two intense peaks at ~532.7 eV ascribed to oxygen double-bonded to carbon (C=O) and oxygen single-bonded to carbon appearing at ~531.5 eV.

Figure 6 displays the results of the deconvolution of the C1s and O1s spectra. The bonds present in the GC samples consist of C=C, C–C, and C=O bonds. Thus, the GC prepared from coconut shell charcoal is dominated by carbon bonds. The content of C=C regions/sp^2 hybridization increases by increasing the reduction temperature. This is possible when the heating temperature increases—then the energy generated for the formation of C=C will also increase, so that the level of sp^2 hybridization increases by increasing temperatures. The C–C component decreases with the reduction temperature, pointing to a lower quantity of sp^3 hybridization. The percentage of oxygen-containing bonds (C=O) tends to decrease. It suggests that the heating process can cause the oxygen bonds to break and form reduced graphene oxide. The releasing of oxygen bonds is known to induce defects in the GC structure, which will be described further in the explanation of Raman spectroscopy. When compared to the XPS spectra from Ref [42, 43], it is obvious that graphene derivatives are mostly composed of C=C sp^2 bonds, with modest contributions from C–C sp^3, C–O, and C=O bonds. The report also mentions the same phenomenon as this study, namely a decrease in the contribution of the C=O group after reduction, including chemical and thermal reduction [42, 43]. Furthermore, the sp^2/sp^3 ratio increases significantly, indicating that the majority of the oxygen-containing functional groups are removed due to the heat treatment. A pristine rGO is sp^2 bonded, which forms a 2-dimensional series in a hexagonal lattice, while carbon with sp^3 bonds tends to form a 3-dimensional tetrahedral structure. In this work, the GC was produced with a mixed sp^2 and sp^3 bonds, which also means a mixture of 2D and 3D structures. Thus, it is suggested that the GC has a mesostructure, which is probably much different from the nanostructure.

GC samples were also subjected to Raman spectroscopy in order to further understand their graphitic and defect structures. The Raman spectra of the GC samples are displayed in Figure 7. It shows two main peaks that are characteristic of the D- and G-bands. The D- and G-peaks were observed at 1344 and 1503 cm^{-1}, respectively. Specifically, the D band is linked with defects in the structure (A_{1g} mode), while the G band is associated with E_{2g} phonon scattering due to the sp^2 hybrid structure

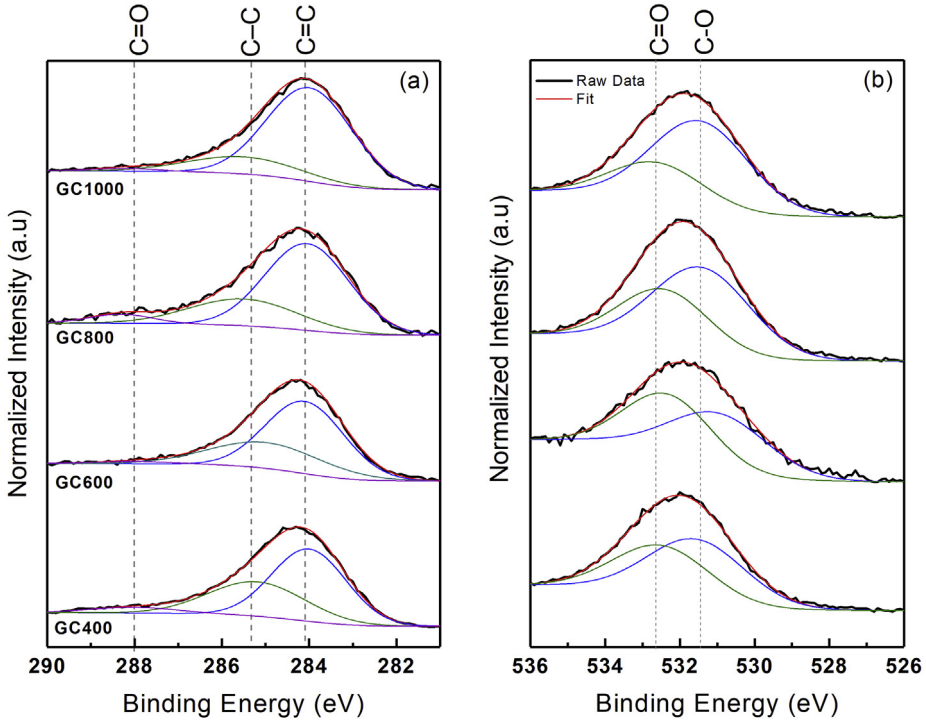

Figure 5. High-resolution XPS spectra of the (a) C1s (b) O1s core level peak.

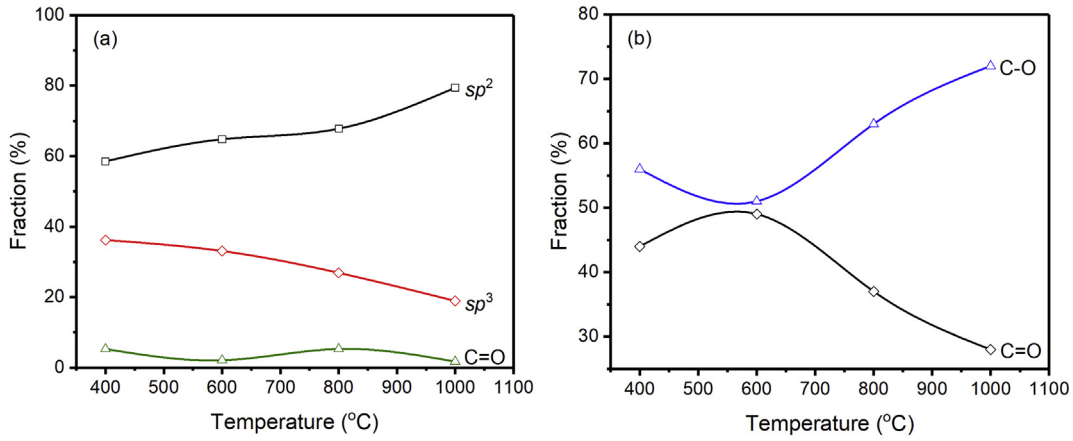

Figure 6. Carbon constituents of the deconvoluted (a) C1s and (b) O1s core level peak. The use of solid lines aims for eye guidance.

[44, 45]. Additionally, the intensity ratio of the D and G peaks (I_D/I_G) in all samples was calculated, which indicates that the I_D/I_G increases as the heating temperature increases. Therefore, GC1000 has the highest I_D/I_G value, indicating that it has more defects or disorders than the other samples [46]. These defects can be in the form of vacancy defects due to the release of oxygen bonds in the structure, as well as line defects and carbon adatoms [47, 48]. The presence of an apparent 2D-peak at 2750 cm^{-1} indicates that a two-dimensional structure has formed on the GC samples [17, 46] which is getting more intense as the temperature increases. In comparison to standard graphene, which is synthesized from graphite using a modified Hummers' method, graphene oxide has an obvious D-peak with an intensity proportional to the G-peak [42, 44, 46]. It differs from pristine graphene, which shows a lower intensity of the D peak. It implies that graphene oxide has more structural defects than pristine graphene [46]. A similar issue occurs with GC samples, in which the GC exhibits increasing structural disorders due to defects, oxygen functional groups, and reconstruction of 2D structures as the heating temperature increases. The GC samples exhibit a higher defect rate when compared to derived standard graphene materials reported by A. Ganguly et al. [46].

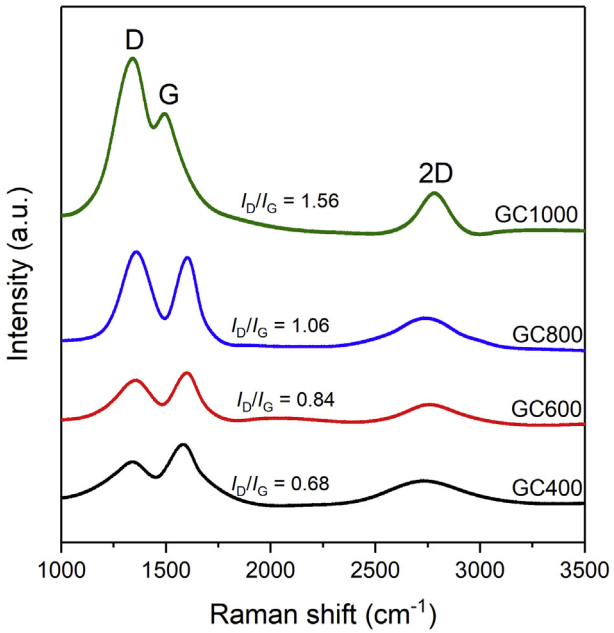

Figure 7. Raman spectra of the GC samples.

The BET surface area analysis technique is extremely effective at determining the porosity and specific surface area of materials. The Barrett-Joyner-Halenda (BJH) method was used to estimate the pore size distribution [49, 50]. The result reveals that the number of pores in GC400 is significantly higher than that in GC1000, with the majority of the pores measuring greater than 2 nm, although there are also some pores that are 1–2 nm in size. On the other hand, GC1000 contains pores of a size greater than 10 nm, but in relatively lower quantities than GC400. As a result, the total pore volume of GC400 and GC1000 were calculated to be 0.09 and 0.04 cc/g, respectively. The pore distribution explicitly indicates that the GC is composed of meso- and micro-pore structures [51, 52, 53, 54]. The GC400 shows greater specific surface area and total pore volume than that of the GC1000. From these results, it can be concluded that the heating process results in an increase in pore size and a decrease in the specific surface area and total pore volume of the material, as shown in Table 1. This tendency is consistent with XRD data, which shows that crystallization increases as the heating temperature rises. According to the XPS data described earlier, increasing the heating temperature results in an increase in sp^2 bonds and a decrease in sp^3 bonds. The sp^3 bonds can be associated with the diamond-*like* structure, while sp^2 bonds can be associated with the graphite-*like* structure. According to a study conducted by P.T. Moseley et al. [55], diamond has a higher density than graphite, which means it has the opposite porosity feature. This is consistent with the results of this study, which indicate that the higher sp^2 content in the sample results in greater pore size. The GC1000 contains higher sp^2 bonds than the GC400, resulting in a greater pore size.

The surface morphologies of the GC samples are probed using SEM and low-resolution TEM images. The SEM photographs of GC samples (Figure 8) demonstrate the typical structure of GC, which is formed of crumpled spherical shapes along with sheet-like shapes. The GC samples that were heated to a higher temperature were less wrinkled. This could be because the heating increased the spaces between the graphenic layers, resulting in an unfolding structure. Thus, it can be inferred that heat treatments have the potential to effectively exfoliate the obtained GC. TEM images also reveal that the GC consists of graphenic flakes with sizes ranging up to a few nanometers, as presented in Figure 9(a –d). It also shows a surface corrugation in some parts that relate to a localized

Table 1. Total pore volume, pore diameter and specific surface area of the GC400 and GC1000 samples examined by BET technique.

Sample	Total Pore Volume (cc/g)	Pore Diameter (nm)	Specific Surface Area (m^2/g)
GC400	0.09	1.69	122.8
GC1000	0.04	13.20	77.4

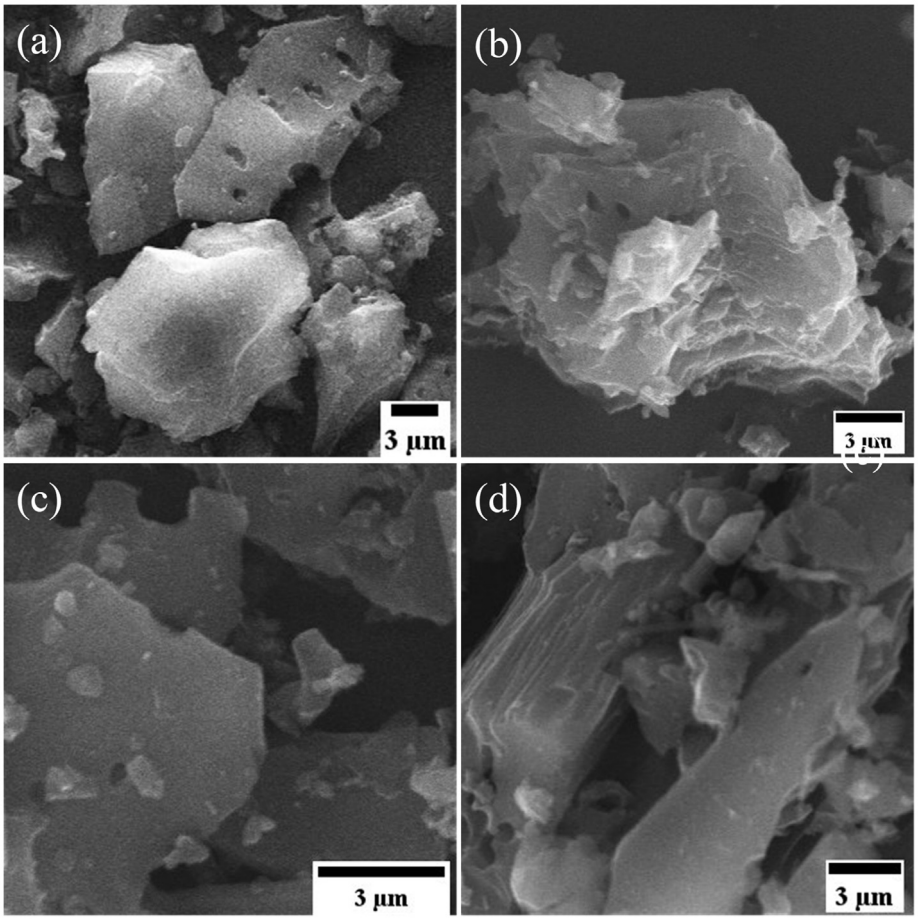

Figure 8. SEM image of the exfoliated GC heated at: (a) 400 °C (b) 600 °C (c) 800 °C, and (d) 1000 °C.

intrinsic strain due to the loading of oxygen functional groups at the graphenic sheets [56]. A comparable microstructure has also been discovered in standard graphene materials by F. J. Sonia and et al. [42], which exhibit the characteristics of folded and crumpled morphology. The corresponding TEM images in their study further reveal that the standard graphene materials are formed of wrinkled graphene sheets. This is consistent with our observations in this work. Furthermore, at a closer view of the TEM images, the basal planes of all GC samples did not show any significant morphological differences. The GC1000 has more crumples and damages at the edges probably because the water removal during the thermal expansion process is harder at 1000 °C and destroys the carbon structure more intensively [24]. However, this fact did not result in a significant change in the XRD pattern. It is clear that the high temperature contributes to the sp^2 network restoration.

Beyond TEM observation, SAXS was employed to quantitatively determine the particle size and shape (form factor) of GC samples. Figure 10 shows the intensities of X-rays scattered by a sample as a function of the scattering angle [34, 57]. SAXS uses the basic principle of Bragg's law in small-angle scattering; the source of high-energy x-rays hit a particle in the sample, then the scattering is detected at a detector with a certain distance. Here, the x-ray energy used in SAXS characterization was 9 keV with a sample-to-detector distance (SDD) of 4.3 m. The use of SDD is very important during the measurement process because it affects the scattering angle used to determine the range of the scattering vector (q). The scattering vector is related to the measured particle size. The long SDD will produce a low q range ($<1\text{nm}^{-1}$), while the low q range represents a larger particle. Meanwhile, the short SDD will produce a high q range ($>1\text{nm}^{-1}$) and represent a smaller particle [58, 59]. In contrast to the SAXS measurements carried out in many previous studies [17, 60, 61], in this study, the measurements were carried out on powder-based samples instead of colloidal states. M. A. Baqiya et al. conducted a preliminary structural study using SAXS with a colloidal solution of graphene as a substance [17]. Compared to our results, the scattering patterns of powder-based samples show steady data compared to that of colloidal-based samples, of which the scattering data are more fluctuating, especially in the lower q range. Moreover, they stated that the Beaucage model is successful in modeling the scattering pattern of the exfoliated graphene-based particle. They also suggested that the exfoliated graphene-based particle formed a spherical shape and agglomerated plate-like flakes with a radius in the nanometer order [17]. As an in-depth analysis of SAXS that includes large particles, this work proposes to focus on the analysis using the mass fractal model [62, 63]. The mass fractal model is considered more suitable in representing the structure of the graphene-based materials prepared from coconut shell charcoal. T. M. McCoy and S. Pradhan stated that the mass fractal function is suitable for quantifying the 2- and 3-dimensional structures present in graphene-based structure [60, 61].

In Figure 10, the scattering profile for GC samples shows two structural levels. At each level, the GC samples show a mass fractal regime which illustrates both 3-dimensional structure in lower q range and 2-dimensional structure in higher q range. The illustration model in Figure 10 is used to describe the two structural levels stated. The first level illustrates a crumpled paper sheet in 3-dimensional form. When a crumpled 3-dimensional lump is stretched, the series of 2-dimensional

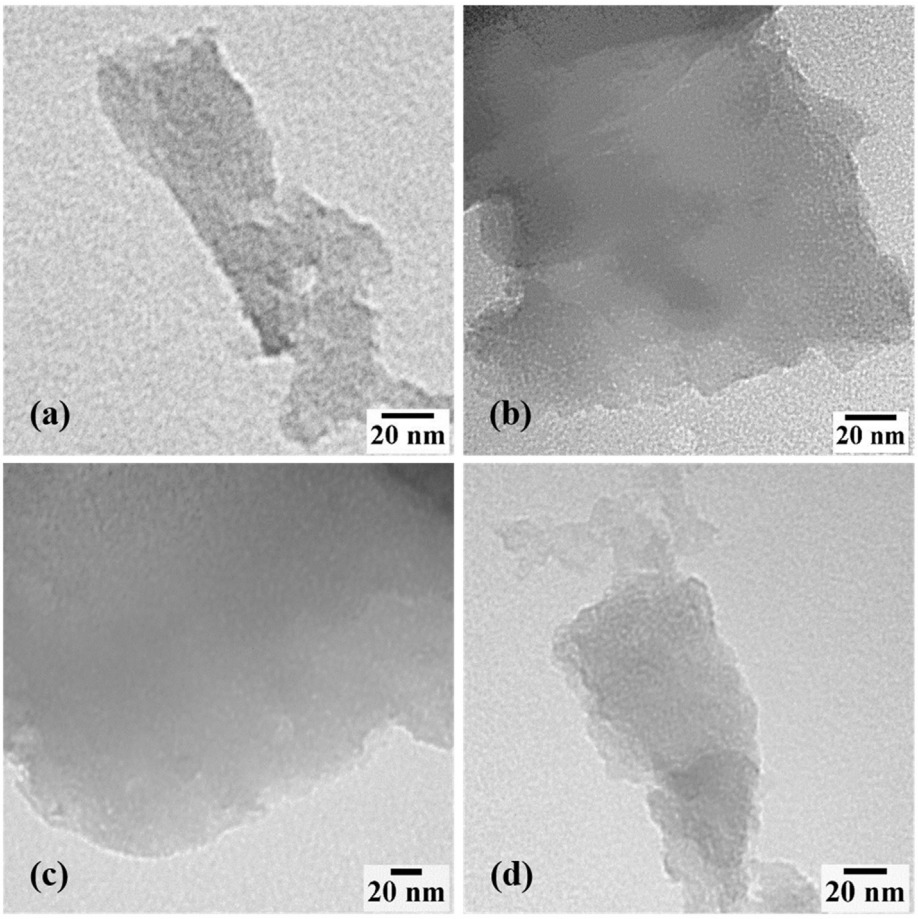

Figure 9. TEM image of the exfoliated GC heated at: (a) 400 °C (b) 600 °C (c) 800 °C, and (d) 1000 °C.

sheets will be seen. These 2-dimensional sheets are called persistence sheets, as they are the primary structure arranging the building block of the crumpled 3D sheet [61].

In order to model the scattering GC samples, a mass fractal model was preferred. The mass fractal model estimates the scattering of inhomogeneous substances according to the power law as $I(q) \propto q^{-\alpha}$, which allows for the determination of the fractal dimensions (D_m) of the material. D_m can provide information about the complexity of the structure, where higher D_m indicates higher complexity [60, 62, 64]. The information about the fractal dimensionality can be obtained by determining

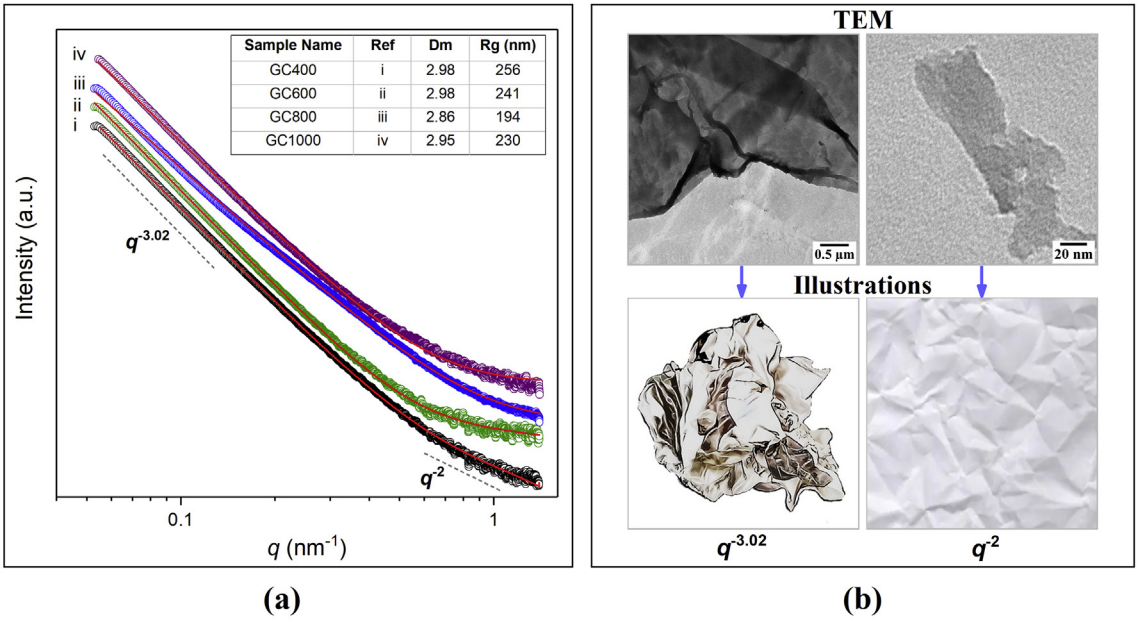

Figure 10. (a) SAXS profiles of the GC samples, and (b) illustrations showing the fractal dimensions compared to TEM images.

the slope of the SAXS scattering intensity profile in the low q range as power law function [63]. 3D objects show the slope $\alpha = 3$ or higher, while 2D objects show the slope $\alpha = 2$. The observed slope for GC400, GC600, GC800, and GC1000 is in the range of 3.02–3.14, indicating the presence of aggregates or 3D objects [29]. N. Singh et al. in their report combined SANS and SAXS profiles to analyze the structure of graphene materials [65]. The SANS and SAXS profiles shown are similar to the SAXS profiles for the GC samples. The scattering experiment shows the presence of branching of the rGO cluster with the incorporation of nanoparticles. The fitting results show that the graphene fractal dimensions range from 2.1 to 3.0 depending on the preparation process [65]. Figure 10 presents the successful fitting curve of the GC samples using mass fractal model, as written in Eq. (1). This model was used to examine the structural quantification of GC samples.

$$I(q) = \frac{\sin[(D_m - 1)\, tan^{-1}(q\xi)]}{(D_m - 1)q\xi\left(1 + q^2\xi^2\right)^{(D_m-1)/2}} \quad (1)$$

where $\xi^2 = 2R_g^2 / D_m(D_m + 1)$, $I(q)$ describes the scattering intensity as a function of the wave vector q, D_m defines the dimension of mass fractal, which must be a value between 0 and 6, and describes the fractal complexity. The parameter ξ is the cut-off length, which is a measure of the linear size of the aggregate or cluster proportional to the radius of gyration R_g. R_g is the radius of gyration of the aggregate or cluster [60].

TEM images show a good agreement with the SAXS observation. It shows that the GC is composed of crumpled-like particles randomly arranged on the surfaces and tending to form the fractal structure with a size in the order of 200 nm. The size of the gyration radius (R_g) of the particles and the shape of the particles were determined quantitatively through curve fitting using the Sasfit program. This process aims to quantitatively determine the size of the particle radius and the shape of its dimensions by matching the curve of the selected model with the curve of the measurement data. Table inserts in Figure 10 display the R_g and D_m of each material calculated using the mass fractal equation. It shows that the particles have a rough shape and are irregularly arranged. Here, the results reveal the change in radius of gyration with respect to heating temperatures. R_g tends to decrease with the increase in heating temperatures in the GC powders, meaning that there is a combination of 2D and 3D structures.

4. Conclusions

In summary, the GC synthesized from old coconut shells, using thermal and chemical exfoliation techniques, has been successfully prepared. The WAXS analysis shows Braggs peaks corresponding to rGO single phase, with the main broad peak appearing at $2\theta \sim 23^{o}$ corresponding to the (002) plane and less intensity peak at $2\theta \sim 43^{\circ}$ corresponding to the (100) plane. The FTIR and XPS investigations reveal that the main bonds in the GC samples are C=C (carbon with sp^2 hybridization), C–C (carbon with sp^3 hybridization), and C=O bonds. As the temperature increases, the oxygen-containing bonds decrease and are suggested to create defects in the GC structure along with the reconstruction of the 2D structure. Raman spectroscopy further demonstrates that as the heating temperature increases, the GC exhibits increased structural disorder due to defects, oxygen functional groups, and reformation of 2D structures. Qualitatively, TEM images shows unique sheet-like smooth waves and crumpled surface with the size up to 250 nm. The result is in good agreement with the result of SAXS analysis, in which the R_g obtained is suggested to have a radius in the order of 200 nm. The SAXS fitting reveals that the structure of GC contains a mixture of 2D and 3D structures, which is confirmed by TEM and XPS. As a final point, the GC powder suggests a mesostructure. Due to their superior physical properties and comprehensive structural characterizations, the obtained GC is expected to contribute in potential applications, such as in the fields of microwave absorption devices and lithium ion battery cathodes.

Declarations

Author contribution statement

Deril Ristiani: Conceived and designed the experiments; Performed the experiments, Wrote the paper.

Retno Asih, Malik Anjelh Baqiya: Analyzed and interpreted the data; Wrote the paper.

Fahmi Astuti: Contributed reagents, materials, analysis tools or data.

Chonthicha Kaewhan, Sarayut Tunmee, Hideki Nakajima, Siriwat Soontaranon: Performed the experiments; Analyzed and interpreted the data.

Darminto: Conceived and designed the experiments; Wrote the paper.

Funding statement

This work was supported by Kementerian Riset Teknologi Dan Pendidikan Tinggi Republik Indonesia (1286/PKS/ITS/2020) and the scholarship granted by the PMDSU Program (D.R.).

Data availability statement

Data included in article/supplementary material/referenced in article.

Declaration of interests statement

The authors declare no conflict of interest.

Additional information

No additional information is available for this paper.

Acknowledgements

The authors wish to express their gratitude to F. M. Wachid for assisting in the preparation of TGA-DTG data for this work.

References

[1] A.K. Geim, K.S. Novoselov, The rise of graphene, Nat. Mater. 6 (2007) 183–191.
[2] S. Pei, H.-M. Cheng, The reduction of graphene oxide, Carbon 50 (2012) 3210–3228.
[3] M.O. Danilov, I.A. Slobodyanyuk, I.A. Rusetskii, G.Y. Kolbasov, Reduced graphene oxide: a promising electrode material for oxygen electrodes, J. Nanostruct. Chem. 3 (2013) 49.
[4] S. Park, J. An, J.R. Potts, A. Velamakanni, S. Murali, R.S. Ruoff, Hydrazine-reduction of graphite- and graphene oxide, Carbon 49 (2011) 3019–3023.
[5] M. Pumera, Graphene-based nanomaterials for energy storage, Energy Environ. Sci. 4 (2011) 668–674.
[6] E. Suarso, F.A. Setyawan, A. Subhan, M.M. Ramli, N.S. Ismail, M. Zainuri, Z. Arifin, D. Darminto, Enhancement of LiFePO4 (LFP) Electrochemical Performance through the Insertion of Coconut Shell Derived rGO–like Carbon as Cathode of Li-Ion Battery, 2021.
[7] F. Yavari, N. Koratkar, Graphene-based chemical sensors, J. Phys. Chem. Lett. 3 (2012) 1746–1753.
[8] S. Rasul, A. Alazmi, K. Jaouen, M.N. Hedhili, P.M.F.J. Costa, Rational design of reduced graphene oxide for superior performance of supercapacitor electrodes, Carbon 111 (2017) 774–781.
[9] M. Czerniak-Reczulska, A. Niedzielska, A. Jędrzejczak, Graphene as a material for solar cells applications, Adv. Mater. Sci. 15 (2015) 67–81.
[10] A.V. Munde, B.B. Mulik, P.P. Chavan, B.R. Sathe, Enhanced electrocatalytic activity towards urea oxidation on Ni nanoparticle decorated graphene oxide nanocomposite, Electrochim. Acta 349 (2020) 136386.
[11] M. Pramanik, C. Li, Y.V. Kaneti, Y. Yamauchi, A mesoporous tin phosphate–graphene oxide hybrid toward the oxygen reduction reaction, Chem. Commun. 53 (2017) 5721–5724.
[12] A.F. Kurniawan, M.S. Anwar, K. Nadiyyah, M. Mashuri, T. Triwikantoro, D. Darminto, Thickness optimization of a double-layered microwave absorber combining magnetic and dielectric particles, Mater. Res. Express 8 (2021) 65001.
[13] A.F. Kurniawan, K. Nadiyyah, M.S. Anwar, R.A. Ajiesastra, Chemical exfoliation and microwave absorption of reduced graphene oxide synthesized from old coconut shells, in: Journal of Physics: Conference Series, IOP Publishing, 2021, p. 12003.

[14] H.J. Yoo, Y.G. Li, W.Y. Cui, W. Chung, Y.-B. Shin, Y.-S. Kim, C. Baek, J. Min, Discrimination and isolation of the virus from free RNA fragments for the highly sensitive measurement of SARS-CoV-2 abundance on surfaces using a graphene oxide nano surface, Nano Convergence 8 (2021) 31.

[15] D. Darminto, R. Asih, Kurniasari, M.A. Baqiya, S. Mustofa, S. Suasmoro, T. Kawamata, M. Kato, I. Watanabe, Y. Koike, Enhanced magnetism by temperature induced defects in reduced graphene oxide prepared from coconut shells, IEEE Trans. Magn. 54 (2018) 1–5.

[16] R. Asih, E.B. Yutomo, D. Ristiani, M.A. Baqiya, T. Kawamata, M. Kato, I. Watanabe, Y. Koike, Darminto, comparative study on magnetism of reduced graphene oxide (rGO) prepared from coconut shells and the commercial product, Inside MS 966 (2019) 290–295.

[17] M.A. Baqiya, A.Y. Nugraheni, W. Islamiyah, A.F. Kurniawan, M.M. Ramli, S. Yamaguchi, Y. Furukawa, S. Soontaranon, E.G.R. Putra, Y. Cahyono, Darminto Risdiana, Structural study on graphene-based particles prepared from old coconut shell by acid–assisted mechanical exfoliation, Adv. Powder Technol. (2020). S0921883120300935.

[18] D. Ristiani, R. Asih, N.S. Puspitasari, M.A. Baqiya, Risdiana, M. Kato, Y. Koike, S. Yamaguchi, Y. Furukawa, Darminto, Introduction of Na^+ in reduced graphene oxide prepared from coconut shells and its magnetic properties, IEEE Trans. Magn. 56 (2020) 1–6.

[19] W. Yang, G. Chen, Z. Shi, C.-C. Liu, L. Zhang, G. Xie, M. Cheng, D. Wang, R. Yang, D. Shi, Epitaxial growth of single-domain graphene on hexagonal boron nitride, Nat. Mater. 12 (2013) 792–797.

[20] B. Pollard, Growing Graphene via Chemical Vapor Deposition, Pomona College, Claremont, CA, USA, 2011.

[21] X. Mei, X. Meng, F. Wu, Hydrothermal method for the production of reduced graphene oxide, Phys. E Low-dimens. Syst. Nanostruct. 68 (2015) 81–86.

[22] S. Farah, A. Farkas, J. Madarász, K. László, Comparison of thermally and chemically reduced graphene oxides by thermal analysis and Raman spectroscopy, J. Therm. Anal. Calorim. 142 (2020) 331–337.

[23] A. Nugraheni, M. Nashrullah, F. Prasetya, F. Astuti, D. Darminto, Study on Phase, Molecular Bonding, and Bandgap of Reduced Graphene Oxide Prepared by Heating Coconut Shell, 2015, p. 285.

[24] A.V. Dolbin, M.V. Khlistyuck, V.B. Esel'son, V.G. Gavrilko, N.A. Vinnikov, R.M. Basnukaeva, I. Maluenda, W.K. Maser, A.M. Benito, The effect of the thermal reduction temperature on the structure and sorption capacity of reduced graphene oxide materials, Appl. Surf. Sci. 361 (2016) 213–220.

[25] C. Zhou, H. Li, W. Zhang, J. Li, S. Huang, Y. Meng, J. deClaville Christiansen, D. Yu, Z. Wu, S. Jiang, Direct investigations on strain-induced cold crystallization behavior and structure evolutions in amorphous poly (lactic acid) with SAXS and WAXS measurements, Polymer 90 (2016) 111–121.

[26] H. Zhao, Q. Zhang, S. Ali, L. Li, F. Lv, Y. Ji, F. Su, L. Meng, L. Li, A real-time WAXS and SAXS study of the structural evolution of LLDPE bubble, J. Polym. Sci. B Polym. Phys. 56 (2018) 1404–1412.

[27] Z. Shen, J. Li, M. Yi, X. Zhang, S. Ma, Preparation of graphene by jet cavitation, Nanotechnology 22 (2011) 365306.

[28] L. Costa, A. Andriatis, M. Brennich, J.-M. Teulon, S.W. Chen, J.-L. Pellequer, A. Round, Combined small angle X-ray solution scattering with atomic force microscopy for characterizing radiation damage on biological macromolecules, BMC Struct. Biol. 16 (2016) 18.

[29] S. Pradhan, Quantification of Graphene Oxide Structure Using an Improved Model, PhD Thesis, University of Cincinnati, 2012.

[30] C. Nita, B. Zhang, J. Dentzer, C.M. Ghimbeu, Hard carbon derived from coconut shells, walnut shells, and corn silk biomass waste exhibiting high capacity for Na-ion batteries, J. Energy Chem. 58 (2021) 207–218.

[31] C. Tangsathitkulchai, S. Junpirom, J. Katesa, Carbon dioxide adsorption in nanopores of coconut shell chars for pore characterization and the analysis of adsorption kinetics, J. Nanomater. (2016) 2016.

[32] Y. Fan, G.D. Fowler, C. Norris, Potential of a pyrolytic coconut shell as a sustainable biofiller for styrene–butadiene rubber, Ind. Eng. Chem. Res. 56 (2017) 4779–4791.

[33] T. Rout, D. Pradhan, R.K. Singh, N. Kumari, Exhaustive stu§33a ESDXdy of products obtained from coconut shell pyrolysis, J. Environ. Chem. Eng. 4 (2016) 3696–3705.

[34] S. Musyarofah, W. Soontaranon, Triwikantoro Limphirat, S. Pratapa, XRD, WAXS, FTIR, and XANES studies of silica-zirconia systems, Ceram. Int. 45 (2019) 15660–15670.

[35] S.N.H. Abbandanak, H. Aghamohammadi, E. Akbarzadeh, N. Shabani, R. Eslami-Farsani, M. Kangooie, M.H. Siadati, Morphological/SAXS/WAXS studies on the electrochemical synthesis of graphene nanoplatelets, Ceram. Int. 45 (2019) 20882–20890.

[36] F.W. Low, C.W. Lai, S.B. Abd Hamid, Easy preparation of ultrathin reduced graphene oxide sheets at a high stirring speed, Ceram. Int. 41 (2015) 5798–5806.

[37] M. Enayati, A. Nemati, A. Zarrabi, M.A. Shokrgozar, The role of oxygen defects in magnetic properties of gamma-irradiated reduced graphene oxide, J. Alloys Compd. 784 (2019) 134–148.

[38] O.J. Guy, K.-A.D. Walker, Silicon carbide biotechnology, in: Chapter 4 - Graphene Functionalization for Biosensor Applications, second ed., Elsevier, 2016, pp. 85–141.

[39] J. Lefebvre, F. Galli, C.L. Bianchi, G.S. Patience, D.C. Boffito, Experimental methods in chemical engineering: X-ray photoelectron spectroscopy-XPS, Can. J. Chem. Eng. 97 (2019) 2588–2593.

[40] A.P. Savintsev, Y.O. Gavasheli, Z.K. Kalazhokov, K.K. Kalazhokov, X-ray photoelectron spectroscopy studies of the sodium chloride surface after laser exposure, J. Phys.: Conf. Ser. 774 (2016) 12118.

[41] C.-H. Chuang, Chemical Modification of Graphene Oxide by Nitrogenation: an X-ray Absorption and Emission Spectroscopy Study, Scientific Reportsat. (n.d.) 10.

[42] F.J. Sonia, H. Kalita, M. Aslam, A. Mukhopadhyay, Correlations between preparation methods, structural features and electrochemical Li-storage behavior of reduced graphene oxide, Nanoscale 9 (2017) 11303–11317.

[43] S.-W. Kim, H.-K. Kim, S. Lee, K. Lee, J.T. Han, K.-B. Kim, K.C. Roh, M.-H. Jung, New approach to determine the quality of graphene, ArXiv Preprint ArXiv:1709.09879 (2017).

[44] S. Qin, X. Guo, Y. Cao, Z. Ni, Q. Xu, Strong ferromagnetism of reduced graphene oxide, Carbon 78 (2014) 559–565.

[45] F. Tuinstra, J.L. Koenig, Raman spectrum of graphite, J. Chem. Phys. 53 (1970) 1126–1130.

[46] A. Ganguly, S. Sharma, P. Papakonstantinou, J. Hamilton, Probing the thermal deoxygenation of graphene oxide using high-resolution in situ X-ray-based spectroscopies, J. Phys. Chem. C 115 (2011) 17009–17019.

[47] W. Tian, W. Li, W. Yu, X. Liu, A review on lattice defects in graphene: types, generation, effects and regulation, Micromachines 8 (2017) 163.

[48] J. Tuček, P. Błoński, J. Ugolotti, A.K. Swain, T. Enoki, R. Zbořil, Emerging chemical strategies for imprinting magnetism in graphene and related 2D materials for spintronic and biomedical applications, Chem. Soc. Rev. 47 (2018) 3899–3990.

[49] V. Paranthaman, K. Sundaramoorthy, B. Chandra, S.P. Muthu, P. Alagarsamy, R. Perumalsamy, Investigation on the performance of reduced graphene oxide as counter electrode in dye sensitized solar cell applications, Phys. Status Solidi (2018) 1800298.

[50] Z. Li, Z. Liu, Z. Wu, G. Zeng, B. Shao, Y. Liu, Y. Jiang, H. Zhong, Y. Liu, Fabrication of the tea saponin functionalized reduced graphene oxide for fast adsorptive removal of Cd(II) from water, Appl. Phys. A 124 (2018) 398.

[51] O. Oginni, K. Singh, G. Oporto, B. Dawson-Andoh, L. McDonald, E. Sabolsky, Effect of one-step and two-step H3PO4 activation on activated carbon characteristics, Biores. Techn. Reports 8 (2019) 100307.

[52] X. Wang, H. Pan, Q. Lin, H. Wu, S. Jia, Y. Shi, One-step synthesis of nitrogen-doped hydrophilic mesoporous carbons from chitosan-based triconstituent system for drug release, Nanoscale Res. Lett. 14 (2019) 1–12.

[53] V. Ospina, R. Buitrago, D.P. Lopez, HDO del guaiacol mediante el uso de catalizadores NiMo soportados sobre carbón activado obtenido a partir de la torta de higuerilla, Ing. Invest. 35 (2015) 49–55.

[54] L. Feng, Y. Shen, T. Wu, B. Liu, D. Zhang, Z. Tang, Adsorption equilibrium isotherms and thermodynamic analysis of CH_4, CO_2, CO, N_2 and H_2 on NaY Zeolite, Adsorption 26 (2020) 1101–1111.

[55] P.T. Moseley, D.A. Rand, A. Davidson, B. Monahov, Understanding the functions of carbon in the negative active-mass of the lead–acid battery: a review of progress, J. Energy Storage 19 (2018) 272–290.

[56] B. Gupta, N. Kumar, K. Panda, V. Kanan, S. Joshi, I. Visoly-Fisher, Role of oxygen functional groups in reduced graphene oxide for lubrication, Sci. Rep. 7 (2017) 45030.

[57] J. Bolze, V. Kogan, D. Beckers, M. Fransen, High-performance small- and wide-angle X-ray scattering (SAXS/WAXS) experiments on a multi-functional laboratory goniometer platform with easily exchangeable X-ray modules, Rev. Sci. Instrum. 89 (2018) 85115.

[58] A. Nugraheni, D. Jayanti, K. Kurniasari, S. Soontaranon, E. Putra, D. Darminto, Structural analysis on reduced graphene oxide prepared from old coconut shell by Synchrotron X-ray scattering, IOP Conf. Ser. Mater. Sci. Eng. 196 (2017) 12007.

[59] A. Taufiq, Sunaryono, E.G. Rachman Putra, A. Okazawa, I. Watanabe, N. Kojima, S. Pratapa, Darminto, nanoscale clustering and magnetic properties of Mn x Fe3−x O4 particles prepared from natural magnetite, J. Supercond. Nov. Magnetism 28 (2015) 2855–2863.

[60] T.M. McCoy, L. De Campo, A.V. Sokolova, I. Grillo, E.I. Izgorodina, R.F. Tabor, Bulk properties of aqueous graphene oxide and reduced graphene oxide with surfactants and polymers: adsorption and stability, Phys. Chem. Chem. Phys. 20 (2018) 16801–16816.

[61] S. Pradhan, Quantification of Graphene Oxide Structure Using an Improved Model, University of Cincinnati, Cincinnati, 2012.

[62] G.C. Bushell, Y.D. Yan, D. Woodfield, J. Raper, R. Amal, On techniques for the measurement of the mass fractal dimension of aggregates, Adv. Colloid Interface Sci. 95 (2002) 1–50.

[63] K. Malekani, Comparison of techniques for determining the fractal dimensions of clay minerals, Clay Clay Miner. 44 (1996) 677–685.

[64] D.F.R. Mildner, P.L. Hall, Small-angle scattering from porous solids with fractal geometry, J. Phys. D Appl. Phys. 19 (1986) 1535–1545.

[65] N. Singh, J.R. Ansari, M. Pal, A. Das, D. Sen, D. Chattopadhyay, A. Datta, Enhanced blue photoluminescence of cobalt-reduced graphene oxide hybrid material and observation of rare plasmonic response by tailoring morphology, Appl. Phys. A 127 (2021) 1–12.